Progress in Additive Manufacturing
https://doi.org/10.1007/s40964-025-01011-w

FULL RESEARCH ARTICLE

# Influence and handling of process interruptions in PBF-LB of AlSi10Mg

**M. Moser**[1] · **S. Brenner**[1] · **G. Löwisch**[2] · **V. Nedeljkovic-Groha**[1]

Received: 31 October 2024 / Accepted: 5 February 2025


**Abstract**
The high degree of design freedom is a major advantage of additive manufacturing processes and enables the production of highly complex structures that cannot be realized with conventional manufacturing methods. This makes AM processes such as Powder Bed Fusion of Metal with Laser Beam (PBF-LB/M) an attractive option for different industries. However, the production process can be interrupted for various reasons. In addition to a planned pause, e.g., for the production of smart components, various technical issues can lead to an unwanted interruption of the process. In any cases, if the user continues the production process after an interruption, the temperature histories of the produced components and the PBF-LB/M machine are different compared to a non-interrupted process. The literature shows that the cool-down of the system and the components during the process interruption results in various types of component defects. According to our current state of knowledge, the formation of the interruption marks is the most critical defect resulting from a process interruption. Due to the resulting notch effect, the global component properties are often severely impaired even for short interruption times. The easiest way to eliminate the influence of the interruption marks is therefore to remove them by machining the components. An unplanned post-processing using traditional methods like milling or turning is usually difficult or even impossible as the necessary requirements for the component geometry are often not met. In many cases, machining is also not economically viable. In order to address this challenge, three different processing methods were tested in the present study: blasting, vibratory finishing, and manual grinding. These methods are not restricted in the mentioned way and can be used spontaneously to remove the marks quickly and simply. The extent to which the methods affect the surface, the geometry of the interruption marks and the residual stresses was investigated. Fatigue tests were performed to assess the capability of these methods to reduce the negative effects of a process interruption. The results show that the investigated post-processing methods have different effects on the component properties and fatigue strength. All three methods have shown that the negative effects of the interruption marks and thus the scrap rate due to an interruption in the PBF-LB/M can be significantly reduced using appropriate post-processing methods.

**Keywords** Powder bed fusion of metal with laser beam (PBF-LB/M) · AlSi10Mg · Process interruption · Additive manufacturing (AM) · Mechanical properties

## 1 Introduction

Additive manufacturing processes are increasingly being adopted by the industry. This expansion is largely due to the ability to economically produce highly complex structures even in small quantities, thereby enabling new possibilities for lightweight construction concepts and customization. Additionally, these methods typically require fewer manufacturing steps and result in lower material consumption compared to traditional manufacturing techniques, making them more economical and more sustainable. [1, 2]

One of the most widely used techniques for producing metal components is powder bed fusion of metal with laser

✉ M. Moser
martin.moser@unibw.de

[1] Institute for Design and Production Engineering, Department of Mechanical Engineering, University of the Bundeswehr Munich, Werner-Heisenberg-Weg 39, 85577 Neubiberg, Germany

[2] Institute for Weapons Technology and Materials Science, Department of Mechanical Engineering, University of the Bundeswehr Munich, Werner-Heisenberg-Weg 39, 85577 Neubiberg, Germany

Published online: 22 February 2025

beam (PBF-LB/M). In PBF-LB/M, metal powder is locally melted by a focused laser beam, building the components layer by layer. However, the build process can be interrupted for various reasons. In the production of smart components, where sensors or actuators are integrated into a part, this layer-wise build-up can be intentionally paused at a defined layer. The dynamic interactions between the laser beam, the powder bed, the melt pool, and the solidified material make the process highly complex and can lead to unforeseen complications even with meticulous planning resulting in an unplanned process interruption. Whether due to a planned interruption or a technical issue (e.g., power outage, sensor malfunction), the temperature profile of the machine and the components differs from that of a regular build job. Consequently, an interruption can have a significant impact on both the process and the quality of the finished components. The machine downtime causes an economic loss and planning complications. If the build job is canceled, there is also a waste of powder, consumed shielding gas and working hours for example. However, if the build job is continued and completed after the interruption, it is difficult to estimate the impact on the component quality. The system and components cool down during the interruption, leading to a defect known as layer shift and the formation of interruption marks [3]. This defect is illustrated in Fig. 1, which shows a topology-optimized part made of AlSi10Mg, produced by PBF-LB/M. If no post-processing of the components is planned, this defect not only represents a visual flaw, but also leads to a notch effect, which has a negative impact on the mechanical properties, especially for dynamically loaded components in the as-built state. In addition, there might be a risk of weakened bonding between the parts printed before and after the interruption due to an increased porosity or a changed microstructure.

A major disadvantage of additive manufacturing is the low build rate. Depending on the components and process parameters, a build job can take several days or even weeks. For optimal machine utilization, it is therefore often advisable to run long-duration build jobs overnight or over the weekend. However, if the company does not have the capacity to monitor the process 24/7, an unnoticed interruption of several hours or even days becomes more likely. Even if the interruption is noticed by monitoring systems, rectifying such a problem often requires the presence of qualified personnel on site at the machine. Even if the cancelation of a long-term build job is associated with a great economic loss, the implementation of an appropriate working model is probably not profitable, especially for small companies.

The effects of manufacturing interruptions have been examined in the literature before [4–12]. Various scenarios with different interruption durations (ranging from 15 min to 24 h), machine conditions (open/closed build chamber, build plate heating on/off), and materials (aluminum and nickel alloys, Ti-6Al-4 V, steel) have been investigated. Besides a dark discoloration of the interruption level, only a slight change in the microstructure was observed in most of these studies. While some studies have found no significant impact on the mechanical properties [6–10], others have reported contrasting results [4, 5, 11, 12]. These conflicting findings may be attributed to the differing scenarios, materials, and interruption durations considered in each study. However, the previous research has demonstrated that an interruption in the PBF-LB/M process leads to two main types of faults, both related to the cooling of the machine and the components (Fig. 2). For as-built parts where no machining is planned, the already mentioned notch effect of the interruption mark results in a significant reduction of the fatigue strength as shown in Fig. 2a [11, 12]. Even relatively short interruption times of 40 min can cause the formation of the marks [6]. While Binder et al. [6] assume material shrinkage to be the main cause of the layer shift, Moser et al. [12] attribute its formation to the cool-down of the laser optics.

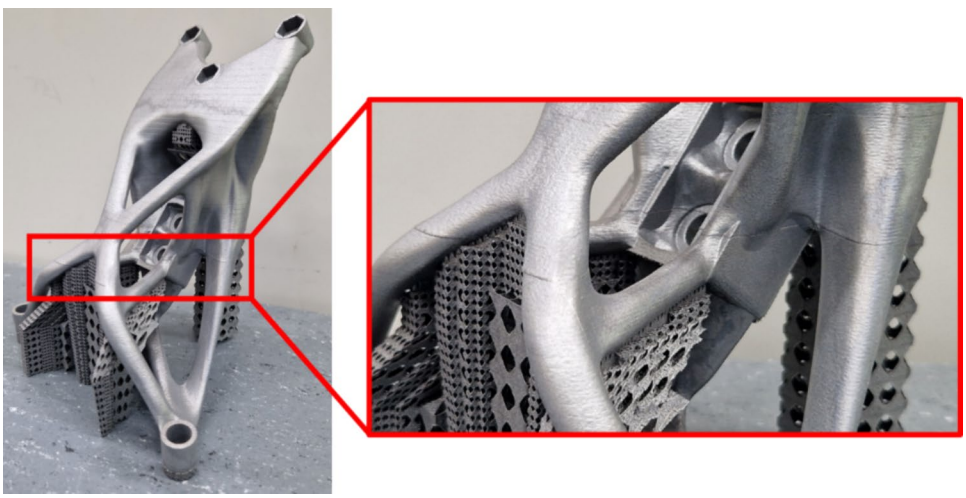

**Fig. 1** Component made of AlSi10Mg fabricated by PBF-LB/M with interruption marks in a critical area as a result of an unplanned process interruption

This leads to a positioning error of the laser spot when continuing the build job, which results in an offset of the part area produced after the interruption and the formation of the interruption marks.

The second defect is an increased porosity in the interruption plane due to a higher layer thickness as a result of thermal shrinkage of the components in the build direction. Depending on the sample geometry and interruption duration, this can cause a higher powder layer thickness when the build job is continued. If the layer thickness or the processing parameters are not adjusted while performing the restart procedure, this leads to an increased risk of pore formation in the interruption area, resulting in a significant rise in the scattering of the fatigue lifetime as shown for machined specimens in Fig. 2b [12]. Based on the current state of knowledge, the influence of the interruption marks appears to be more critical than that of the increased porosity. For this reason, this study focuses on the properties around the marks and their influence on the fatigue strength.

Currently, no study has addressed the question of how to deal with these issues respectively the components affected by an interrupted PBF-LB/M process to reduce the risk of faulty parts and the scrap rate. From the authors' point of view, there are two logical approaches to deal with the mentioned consequences of a process interruption. The first approach is to optimize the restart procedure or to adjust the process parameters when continuing the build job. This can minimize the risk of an increased porosity and a defective connection between the component areas before and after the interruption. This is the subject of further studies and will be published in future. A second approach is the removal of the interruption marks and the associated notch effect. The marks are often more critical than the increased porosity as they negatively affect the mechanical properties in general. Especially under dynamic loads, a significant reduction in the service life of affected components is to be feared. The interruption marks and the pores correspond to a geometric notch, to which the fatigue strength reacts very strongly. Typically, this problem can be resolved by removing the marks through subtractive post-processing methods like milling or turning. However, this approach is generally feasible only for components that were designed with such post-processing in mind as suitable clamping surfaces are required. Additionally, a machining allowance is necessary to ensure that the specified dimensions and the functionality of the component are maintained. Furthermore, the post-processing of highly complex AM structures is often difficult or even impossible with conventional methods [13]. In many cases, machining is also not economically viable. Accordingly, this study examines three post-processing techniques that do not require clamping surfaces or machining allowance: blasting, vibratory finishing and manual grinding. All three of them are simple and relatively fast processes that can be applied with minimal preparations.

In addition to surface inhomogeneities such as roughness, pores or geometric defects, residual stresses also have a significant effect on fatigue strength [14–16]. Literature indicates that post-processing techniques affect not only surface roughness but also residual stresses [14, 17, 18]. At the beginning of the study, it was assumed that each of the investigated processes affects these component properties in different ways. While blasting introduces the highest residual compressive stresses, vibratory finishing generates the lowest surface roughness. However, both processes cannot be expected to completely remove the interruption marks. Among the methods considered, manual grinding is the only method that can completely remove the marks. But the surface finish is very irregular with this process. While blasting and vibratory finishing are well-established methods whose effects have been extensively studied [14, 18–23], manual grinding is a relatively poor investigated process [24].

The aim of the study was to investigate whether the negative effect of an interruption mark can be reduced and how the roughness and residual stresses are affected by a quick and easy post-processing. The effect was evaluated based on the resulting fatigue strength and fracture behavior. The findings are intended to reduce the loss of quality caused by an interruption and thus the scrap rate.

## 2 Materials and methods

In this study, all samples were produced using a standard SLM125HL® system (Nikon SLM Solutions AG, Germany) following the parameters detailed in Table 1. Each build job was started once the base plate reached the necessary temperature of 150 °C and the oxygen level in the build chamber was reduced to 0.05%. The flow rate of the argon shielding gas was maintained at 4 m/s. The AlSi10Mg powder, featuring a particle size distribution of 20 to 63 µm and produced through gas atomization, was supplied by Nikon SLM Solutions AG and utilized in a recycled and sieved state.

The considered scenario was a power outage with a process interruption of 10 h. Throughout the interruption, the build chamber remained closed, thereby preserving the protective gas atmosphere. Furthermore, the base plate heating and the protective gas flow were deactivated. For the investigations, several build jobs were conducted, each consisting of 30 fatigue test specimens conforming to DIN 50113 [25] (Ø14 × 105 mm), printed in z-direction and on a three-millimeter-high volume support (Fig. 3). While the reference samples were produced regularly, the build jobs of the interrupted samples were paused manually in the middle of the cylindrical test area after the exposure of the layer at a specimen height of 52.5 mm.

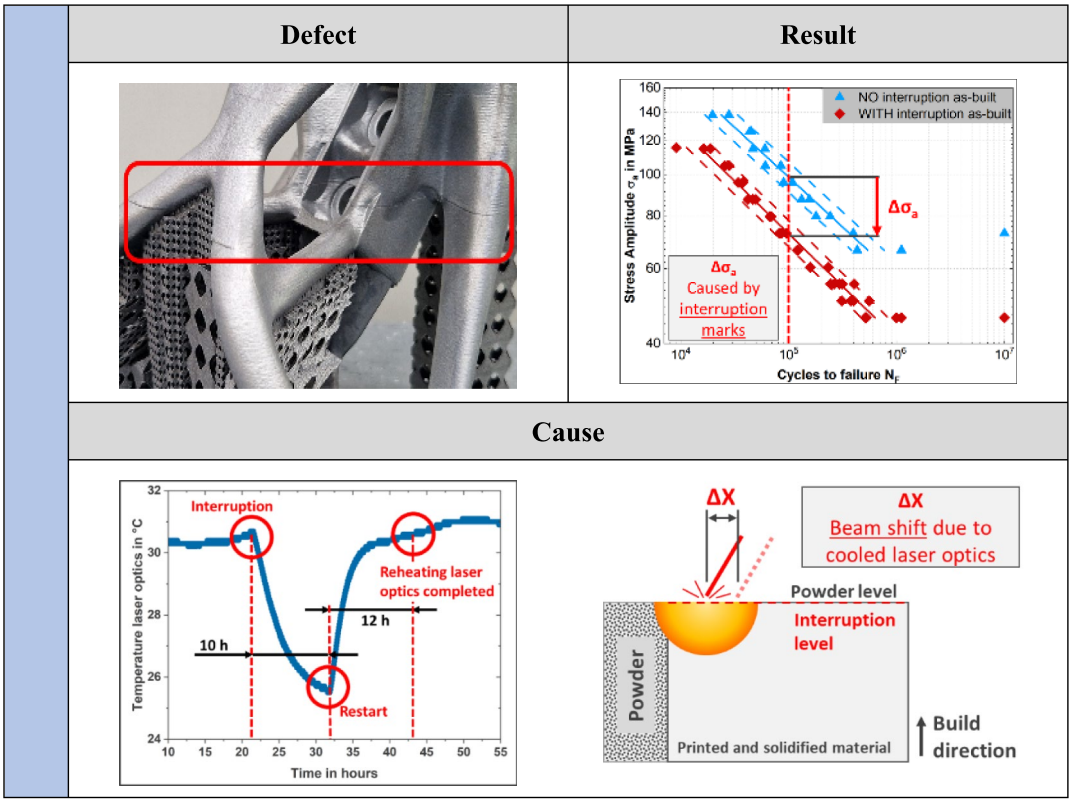
Defect
Result
NO interruption as-built
WITH interruption as-built
Stress Amplitude $\sigma_a$ in MPa
Cycles to failure $N_F$
$\Delta\sigma_a$
$\Delta\sigma_a$ Caused by interruption marks
Cause
Temperature laser optics in °C
Time in hours
Interruption
Reheating laser optics completed
Restart
10 h
12 h
ΔX
ΔX Beam shift due to cooled laser optics
Powder level
Interruption level
Powder
Printed and solidified material
Build direction

*a)*

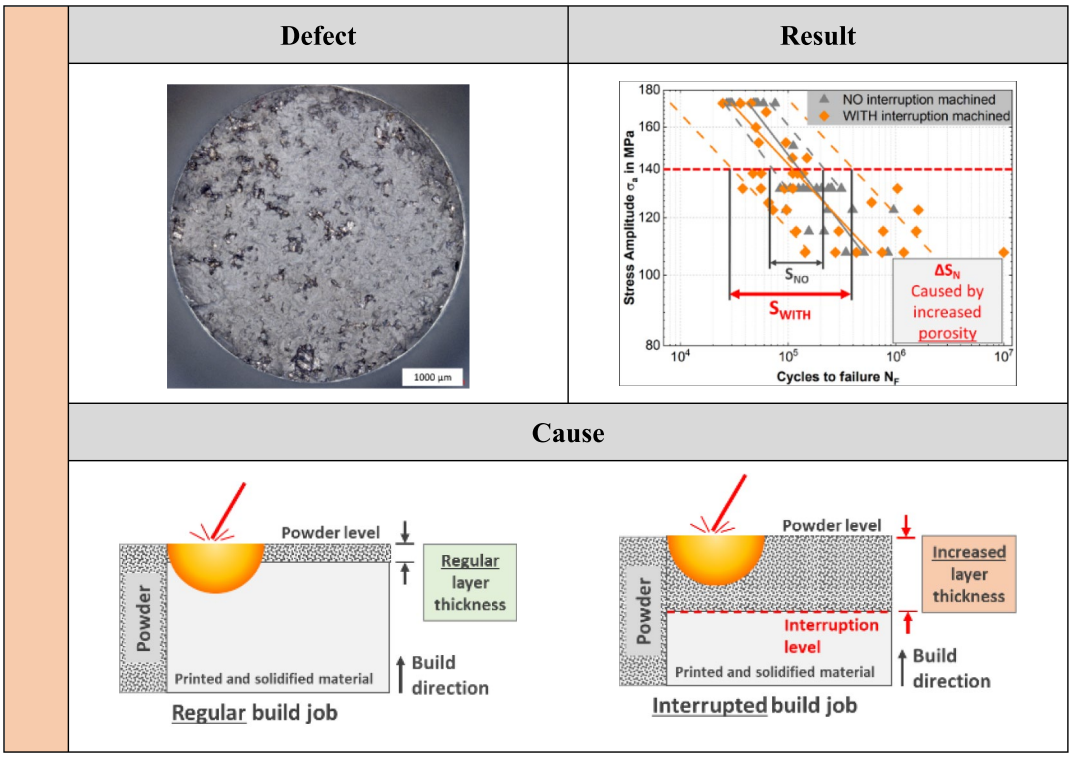
Defect
Result
1000 µm
NO interruption machined
WITH interruption machined
Stress Amplitude $\sigma_a$ in MPa
Cycles to failure $N_F$
$S_{NO}$
$S_{WITH}$
$\Delta S_N$ Caused by increased porosity
Cause
Powder level
Regular layer thickness
Powder
Printed and solidified material
Build direction
Regular build job
Increased layer thickness
Interruption level
Interrupted build job

*b)*

◂**Fig. 2** Critical defects due to an interruption in PBF-LB/M with their results and causes [12]. **a** Interruption marks result in a reduction in fatigue strength due to their notch effect. Their formation is caused by a positioning error of the laser spot as a consequence of the cool-down of the laser optics. **b** More porosity leads to a higher scattering of fatigue life. The reason for this is an increased layer thickness due to the cooling and shrinking of the components

After the planned interruption period of 10 h, the restart procedure used by Moser et al. [12] was carried out. For this purpose, the base plate heating and the inert gas flow were switched on again. After a waiting time of 15 min, several manual recoating processes followed to ensure a uniform powder layer on all samples. The position of the platform remained unchanged. The standard parameters shown in Table 1 were used when continuing the build job. For this purpose, the manually applied powder layer was exposed only once.

After completion, the samples were grouped according to their production conditions (NO or WITH interruption) and the intended post-processing. Afterward, post-processing was carried out using the methods blasting (SB), vibratory finishing (VF), and manual grinding (MG). The samples which were tested in the as-built condition (AB) were not reworked. The properties of the NO_AB samples served as the benchmark for the effect of the interruption and the post-processing methods. Table 2 provides an overview of the sample types and their processing state.

### 2.1 Measurement of surface roughness & profile of the interruption marks

The surface topography and roughness were determined using a VR-5200® 3D profilometer (KEYENCE Corporation, Japan). For this purpose, the area shown in Fig. 3 of five samples per type was scanned using the structured light method. Based on EN ISO 4288 [26] and the recommendation of KEYENCE Corporation, five parallel measuring lines with a length of 12.5 mm, a distance of 0.25 mm and a cut-off value $\lambda_C$ of 2.5 mm were selected for the measurement of the roughness height Rz. For the roughness measurements of the interrupted samples, it was not possible to use the measuring distance recommended in EN ISO 4288 [26] as the interruption marks in the middle of the test area would distort the measured values. However, as it can be assumed that both production conditions (NO/WITH interruption) result in a comparable surface roughness, the values of the samples produced without an interruption are also applied for the interrupted samples. Using the same device and the same samples, measurements were performed to analyze the profile of the interruption marks. For each sample, five parallel lines with a distance of 0.25 mm were used as well. Beforehand, the samples were mechanically marked to ensure an approximately identical orientation during the measurements before and after post-processing.

### 2.2 Measurement of residual stresses

Residual stresses were determined according to EN 15305 standards [27]. For the measurement of residual stresses in the near-surface regions, a D8 Discover® (Bruker Corporation, United States) X-ray diffractometer (XRD) was used. The Cr X-ray tube operated at 35 kV and 40 mA, utilizing a vanadium filter with an absorption factor of 2.48, and a collimator with a diameter of 0.5 mm. The angle between the X-ray source and the Eiger2 R 500 K® multi-mode detector (Dectris AG, Switzerland) was set to $2\theta = 140°$, with a measurement time of 80 s. These settings allowed a measurement depth of approximately 5 µm. The measurements were taken at five different angles and six different positions. Three samples were measured for each specimen variant. For regular printed samples, three measurement points were recorded, while interrupted samples had four measurement points (two before and two after the interruption) as shown in Fig. 3. The $\sin^2\psi$ method was employed to analyze the residual stresses $\sigma_{11}$ longitudinal to the sample axis. These residual stresses are superimposed on the test load and are therefore much more critical than the stresses $\sigma_{22}$ perpendicular to the specimen axis. The analysis was performed using diffraction analysis with Pearson VII peak evaluation and a biaxial stress model, utilizing the software Leptos 7® (Bruker Corporation, United States).

### 2.3 Post-processing

Vibratory finishing, blasting and manual grinding were chosen as post-processing methods as the components to be machined require neither a clamping surface nor a machining allowance. These techniques are well-established, widely available in production facilities, and require minimal preparation. Most post-processing methods, including those used in this study, are limited in in their ability to access the internal structures of complex components. Consequently, this study focuses on open structures where the media or tools can access the relevant surfaces. Chemical or electrochemical methods can also be used for the post-processing of internal or complex structures. However, these are less common, barely remove any material, and do not introduce any residual stresses. For this reason, these methods appear to be less promising for achieving the desired objective of minimizing the negative impact of the interruption mark.

- Vibratory finishing was carried out for two hours in a trough vibrator MMTV-5321® (Müller Mechanik, Germany). Before the process, both the triangle-shaped

**Table 1** PBF-LB/M process parameters for specimen fabrication

| Parameter Set | Laser Power (W) | Scan Speed (mm/s) | Hatch Distance (mm) | Slice Thickness (mm) | Base Plate Temperature (°C) | Scan Strategy (-) | Rotational Angle (°) |
|---|---|---|---|---|---|---|---|
| Hatch | 350 | 1650 | 0.13 | 0.03 | 150 | Stripes | 67 |
| Contour | 300 | 730 | / | | | | |

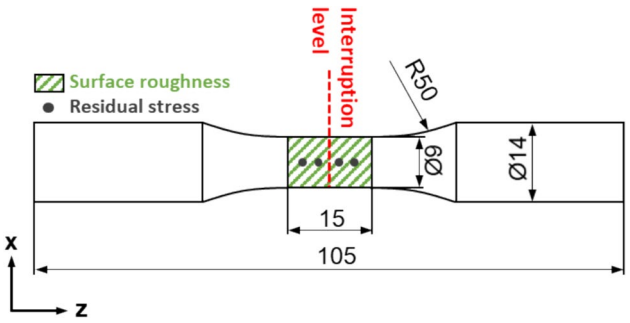


**Fig. 3** Fatigue specimens with marked interruption level and test areas for roughness (green) and residual stress measurements (gray) (units in mm). Build direction along the z-axis

ceramic abrasive media 1010 T® (Hoffmann SE, Germany) and the process water including the added composite SHINY® (Hoffmann SE, Germany) were exchanged to ensure the best possible repeatability.

- For blasting, round glass beads (MHG Strahlanlagen GmbH, Germany) with a grain size of 100–200 µm and a hardness of HRC = 47 were selected, which are well suited for the surface treatment of aluminum components. The samples were processed for 5 min with a blasting pressure of 0.6 MPa. The samples and the blasting nozzle were manually moved at a distance of approximately 3–5 cm. Since this is a very individual process in which the results depend strongly on the operator, the samples were processed by three different individuals to take this factor into account in the best possible way.
- The test area was manually ground using a pneumatic belt sander MBS 20 DH® (joke Technology GmbH, Germany) and an 80-grit corundum sanding belt to remove the interruption marks. As the surface was very rough and uneven, the samples were additionally processed with a fine corundum abrasive fleece. Again, the samples were processed by three people until the test area was uniform and the marks were no longer visible.

Subsequently, all previous measurements (surface topography and roughness, size of the interruption marks, residual stresses) were repeated in order to be able to analyze the changes.

## 2.4 Fatigue tests & fracture analysis

To assess the fatigue strength according to DIN 50100 [28], high-cycle fatigue tests (HCF) were conducted using the pearl string method through rotating bending tests. A Power Rotabend® machine (SincoTec Test Systems GmbH, Germany) was employed for this purpose. The tests were carried out at room temperature and regular environmental conditions, with a load ratio of R = -− 1, and a frequency of 50 to 100 Hz. Depending on the sample type, the load amplitude was modified in a range of 46 to 196 MPa. If a specimen survived $10^7$ cycles undamaged, the test was stopped and the specimen was marked as a runout. For each variant, a minimum of ten fatigue samples were tested. The fracture surfaces of selected samples were examined using a VHX-3000® digital microscope (Keyence Corporation, Japan) and a Zeiss Ultra 55® SEM (Carl Zeiss Microscopy, Germany).

In order to compare defects of different sizes and shapes, the approach by Murakami [29] can be employed. The area of the crack-causing defect corresponds to the Value *´area´* defined by Murakami. A larger *´area´* is associated with a decrease in fatigue strength. The effects of the defect are considered to be equivalent to that of a crack with the length of the square root of the area ($\sqrt{area}$). For a specimen loaded with a stress amplitude of $\sigma_a$ at a load ratio of R = − 1, the range of stress intensity ΔK is given by Eq. (1).

$$\Delta K = Y * 2 * \sigma_a * \sqrt{\pi * \sqrt{area}} \quad (1)$$

For the same load amplitude $\sigma_a$, the stress intensity and thus the fatigue strength depend on the size of the defect, described by $\sqrt{area}$, and the shape factor *Y*. The factor *Y* depends on the position of the defect in relation to the surface. If the defect

**Table 2** Sample types regarding their production conditions (NO/WITH Interruption) and processing state

| | Processing State | | | |
|---|---|---|---|---|
| | As-built | Blasted | Vibratory finished | Manually ground |
| NO Interruption | NO_AB | NO_SB | NO_VF | NO_MG |
| WITH Interruption | WITH_AB | WITH_SB | WITH_VF | WITH_MG |

is located at or near the surface, a $Y$ of 0.65 is selected. For defects in the volume, $Y$ *is* 0.5. This means that the effect of defects near or on the surface is approx. 30% higher than for an equivalent defect in the volume. The distinction as to whether a defect is close to a surface or not is made on the basis of its radius $a$ and the distance between the nearest surface and the center of the defect $h$. With a ratio of $a/h < 0.8$, the defect is considered to be close to the surface. If $a/h > 0.8$, it is a volume defect. Therefore, $Y * \sqrt{area}$ can be used to estimate the effect of a defect based on its size and position.

## 3 Results and discussion

### 3.1 Surface roughness, topography, and size of the interruption marks

Based on the images and 3D scans in Fig. 4 and the values in Table 3, the surface topography and roughness of the sample types can be analyzed. The not post-processed as-built samples (AB) show adhesions of incompletely melted powder particles (Fig. 4a). This is known and significantly influences the surface roughness [14, 17, 21, 22, 30–32]. These satellites were removed by all three post-processing methods tested, which improved the surface quality. The roughness of the as-built samples (AB) was reduced from Rz = 41.2 µm to 29.2 µm by blasting (SB), to 29.5 µm by manual grinding (MG), and to 19.6 µm by vibratory finishing (VF) (Table 3). To evaluate the differences of the post-processing methods, the Rz values were compared using an ANOVA with a significance level of $\alpha = 5\%$. This results in a p-value of $5.8 * 10^{-18}$, which is much smaller than the limit value of 0.05. This reveals that there is a statistically significant difference between the roughness values of the post-processing methods. The blasted samples show a relatively uniform surface structure without obvious elevations or craters, but with many small dimples (Fig. 4b). It is likely that these were caused by the impact of the hard glass beads on the surface and indicate plastic deformation. In contrast, the samples processed by vibratory finishing have a smoother surface overall. However, craters are visible on the surface which appear to be quite deep (Fig. 4c). Initially, the assumption arose that these might be the remaining roughness or profile valleys that could not be completely removed by vibratory finishing, as described by Beevers et al. [13] or Mesicek et al. [22]. On the other hand, Nasab et al. [21] suggested that these craters could also be near-surface defects, such as pores, that have been exposed by vibratory finishing. However, the material removal during vibratory finishing is only slightly larger (0.056 mm in diameter) than with blasting (0.039 mm). In addition, profile measurements show that the craters are up to 30 µm deep, approximately the same depth as the roughness or profile valleys visible in the 3D scans of the AB and SB samples in Fig. 4a and b. Therefore, it seems more likely that the craters are roughness or profile valleys. The surface of the manually ground samples consists of many furrows and peaks and is significantly more uneven compared to the other methods (Fig. 4d). The material removal is with approximately 0.12 mm in diameter the greatest.

Profile curves and images of the interruption marks for each machining condition are shown in Fig. 5. As expected, manual grinding is the only method capable of completely removing the mark (Fig. 5a, g). In the AB state, a rough profile and adhering powder particles are visible (Fig. 5a, d). Blasting and vibratory finishing remove these adhesions and smooth the mark (Fig. 5b, c, e, f). However, this only reduces the size of the mark by 20 µm (Table 3). The smoother profile and the overall lower surface roughness indicate an increased fatigue strength. The images show a significant difference between the blasted (WITH_SB) and the vibratory ground samples (WITH_VF) (Fig. 5e, f). The WITH_SB samples clearly show the dimples that are characteristic of this method, even in the fine corners of the mark. This shows that the small glass beads (grain size 100–200 µm) are able to reach even the small corners of the mark. In comparison, the mark of the vibratory ground samples (WITH_VF) appears much more rugged. This means that the 10 mm abrasive media cannot penetrate as far into the contour of the mark as the much finer glass beads. This suggests a significant difference in the fatigue life of blasted and vibratory finished samples. Furthermore, when analyzing the profile of the as-built samples, it is noticeable that the offset of the marks is not permanent, but slowly disappears with increasing build height. As described by Moser et al. [12], this is probably due to the slow reheating of the laser optics during the course of the build job and the associated reduction in the positioning error of the laser spot as shown in Fig. 2a. The preferred direction of the interruption marks mentioned by Moser et al., which correlates with the direction of the inert gas flow, was also observed in this study.

### 3.2 Residual stress

The residual stresses of the investigated processing states are compared in Fig. 6. The as-built samples produced without interruption (NO_AB) exhibit tensile residual stresses with a mean value of $\sigma_{11} = 137$ MPa. This is related to high-temperature gradients and cooling rates during the process and is of comparable magnitude to literature values [14, 15, 17, 33, 34]. After all post-processing methods, the samples show the presence of residual compressive stresses. This can be explained by the plastic deformation and the resulting hardening of the surface area caused by post-processing and is expected to have a positive effect on fatigue life [14, 16, 17, 21].

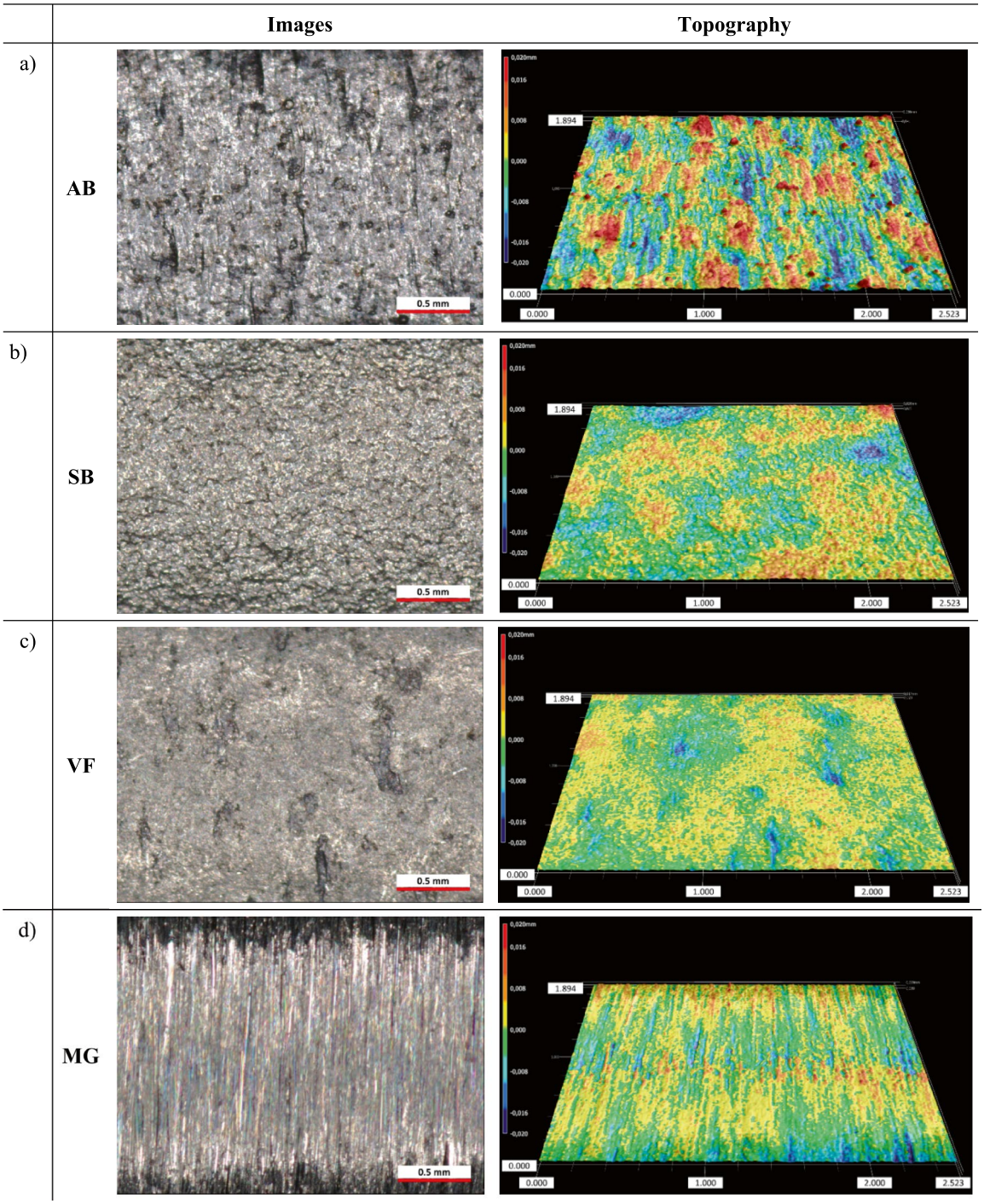


**Fig. 4** Images and topography of the surfaces of the as-built (AB), blasted (SB), vibratory finished (VF), and manually ground (MG) samples

The residual stresses are the greatest after blasting (− 137 to − 143 MPa) (SB), followed by the vibratory finished samples (− 100 to − 119 MPa) (VF). The manually ground samples (MG) exhibit the lowest values with stresses of − 57 to − 97 MPa. Again, an ANOVA was performed to test the significance of the differences between the machining conditions. Both the residual stresses of the regular specimens ($p = 2.3 * 10^{-4}$) and those of the interrupted specimens ($p = 5.4 * 10^{-8}$) differ significantly depending on the post-processing method used. It is also remarkable that, except of the blasted samples, all samples that were produced with an interruption always exhibit lower residual stresses. This might be related to the repeated

**Table 3** Surface roughness Rz and size of the interruption marks of the tested post-processing methods and production conditions

| | AB | | SB | | VF | | MG | |
|---|---|---|---|---|---|---|---|---|
| | NO | WITH | NO | WITH | NO | WITH | NO | WITH |
| Rz (*) (µm) | 41.2 ±8.3 | | 29.2 ±3.3 | | 19.6 ±2.2 | | 29.5 ±6.4 | |
| Size Mark (mm) | / | 0.10 ±0.03 | / | 0.08 ±0.02 | / | 0.08 ±0.01 | / | 0 |

(*) As the interruption marks in the middle of the test area distort the roughness measurements, the samples produced with an interruption could not be tested in accordance with EN ISO 4288. For this reason, roughness values of the same scale are assumed for both manufacturing conditions

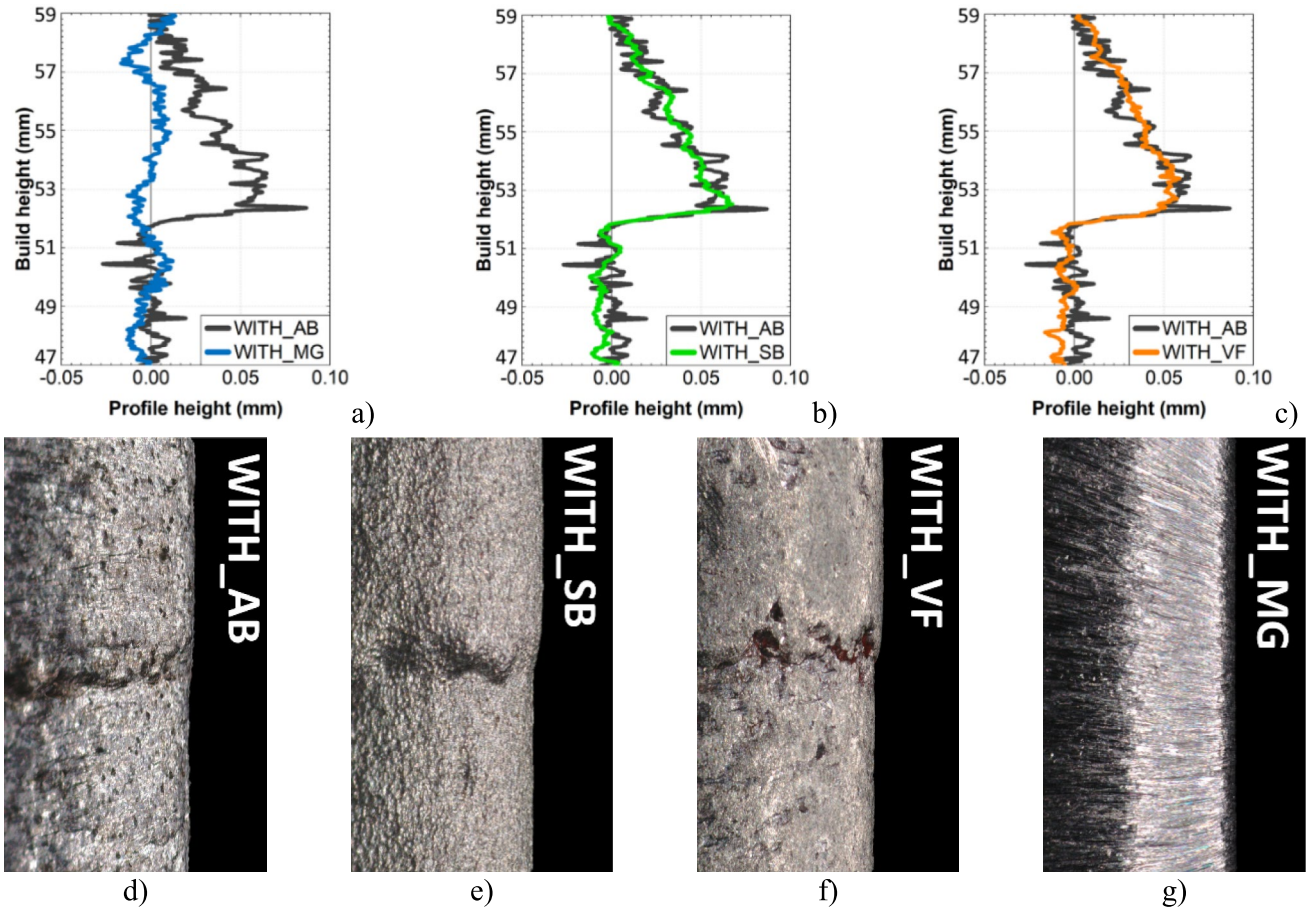


**Fig. 5** Exemplary profile curves and images of the interruption marks in the processing states as-built (WITH_AB), manually ground (WITH_MG), blasted (WITH_SB), and vibratory finished (WITH_VF)

cooling and reheating of the samples during the interruption and the subsequent continuation. The temperature profile is comparable to an uncontrolled heat treatment, which results in a reduction in residual stresses as shown in various studies before [15, 17].

It is conceivable that the residual stresses not only in the interrupted and non-interrupted samples differ, but also in the areas before and after the interruption. In eight out of nine samples, the residual stresses are higher in the area before the interruption than in the area after it. The stresses averaged over all WITH_AB samples were 106 ± 27 MPa before and 95 ± 16 MPa after the interruption. This might be due to the rapid heating that occurs when resuming the build process, which creates higher temperature gradients in the already-cooled section prior to the interruption, thereby leading to increased residual stresses. To evaluate the differences, before post-processing, the residual stresses in the two areas were also compared using an ANOVA with a significance level of $\alpha = 5\%$. This results in a p-value of 0.125, which is greater than the limit value of 0.05. This reveals

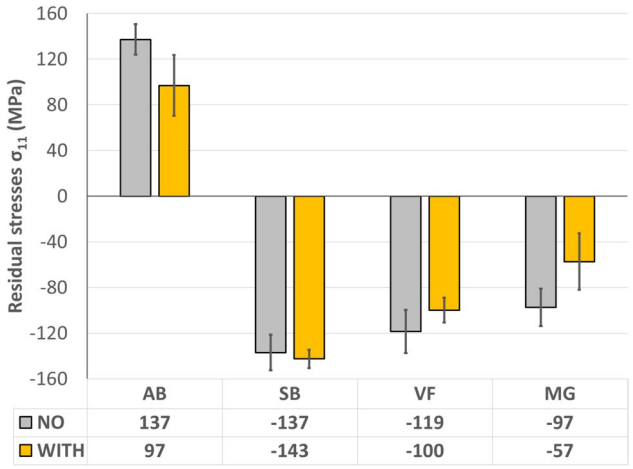


**Fig. 6** Residual stresses for the processing states as-built (AB), blasted (SB), vibratory finished (VF), and manually ground (MG)

that there is no statistically significant difference between the sample areas before and after the interruption. Nevertheless, the frequency of higher residual stresses in the area before the interruption is very conspicuous and offers potential for further investigations.

### 3.3 Fatigue tests

Figure 7 shows the S–N diagram, where the stress amplitude $\sigma_a$ is plotted against the number of cycles to failure $N_F$ on a double logarithmic scale. The diagram includes lines representing crack probabilities of 10%, 50% and 90%. Samples at load levels where cycles of $N_F = 10^7$ have been reached are shown, but have been excluded from the statistical evaluation following DIN 50100 [28]. Samples at load levels below this limit were also excluded. According to DIN 50100, these levels exceed the high-cycle fatigue limit and are not allowed to be evaluated using the pearl string method. The dashed red lines mark a fatigue life of $N_F = 200$k load cycles until failure. Based on this lifetime, the theoretically endurable load amplitudes $\sigma_{a,200\,k}$ of the different sample types can be compared on a quantitative basis. The $\sigma_{a,200\,k}$ values, the gradient of the S–N curve $k$ and the scatter value of the life time $TN$ for the processing states are calculated in accordance with DIN 50100 and listed in Table 4. High values for $\sigma_{a,200\,k}$ and $k$ mean high fatigue strength, whereas a low $TN$ value stands for low scatter and therefore high reproducibility. However, it should be noted that the scatter increases with the gradient. This makes it difficult to compare S–N curves with very different gradients.

Figure 7a compares the fatigue properties of the specimens produced without an interruption (NO). The regularly printed samples in the as-built state (NO_AB) serve as the benchmark. As the previous results already suggested, all post-processing methods have a positive effect on fatigue life. Blasting (SB) more than doubles the theoretically endurable stress amplitude for $N_F = 200$k load cycles from $\sigma_{a,200\,k} = 80$ MPa to 185 MPa. In addition, the S–N curve has a less steep gradient ($k,AB = 3.7$, $k,SB = 9.5$), which also indicates a higher fatigue strength. This is the result of the lower surface roughness and the existing residual compressive stresses. A smaller increase can be seen after vibratory finishing (VF). Here, the bearable load amplitude increases

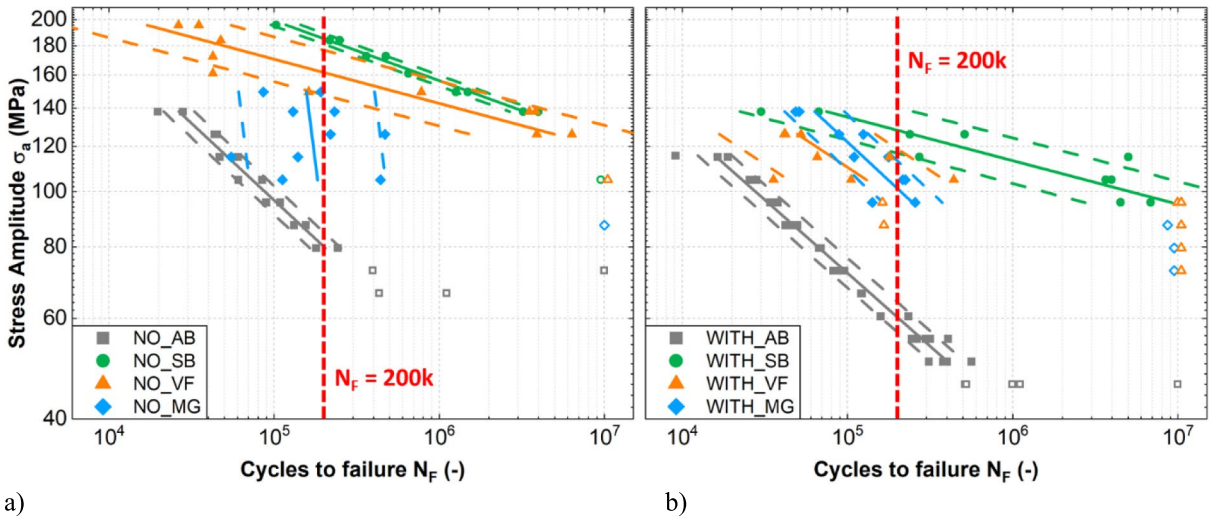


**Fig. 7** S–N diagram for specimens produced without (**a**) and with an interruption (**b**) in the machining conditions as-built (AB), blasted (SB), vibratory finished (VF), and manually ground (MG), including a crack probability of 10% and 90% (dashed lines) and 50% (solid lines). The dashed red lines indicate a fatigue life of NF = 200k. Open symbols represent load levels with runouts which were not considered for the statistical analysis

**Table 4** Fatigue strength $\sigma_{a,200\,k}$, scatter value of the life time TN and the inclination of the S–N curve k, for specimens manufactured without (NO) and with an interruption (WITH) in the tested machining conditions as-built (AB), blasted (SB), vibratory finished (VF), and manually ground (MG)

| | | AB | | SB | | VF | | MG | |
|---|---|---|---|---|---|---|---|---|---|
| | | NO | WITH | NO | WITH | NO | WITH | NO | WITH |
| $\sigma_{a,200\,k}$ | (MPa) | 80 | 60 | 185 | 128 | 161 | 97 | 85 | 101 |
| k | (-) | 3.7 | 3.9 | 9.5 | 13.1 | 12.9 | 5.3 | 0.4 | 3.7 |
| TN | (-) | 1.5 | 1.6 | 1.5 | 11.2 | 10.4 | 8.8 | 6.7 | 2.3 |

to $\sigma_{a,200\,k} = 161$ MPa. While the inclination is even flatter than that for the blasted samples ($k,VF = 12.9$), the scattering is significantly greater with $TN,VF = 10.4$. In addition to the lower residual compressive stresses, the valleys shown in Fig. 4c appear to be the most likely reason for this. After the roughness was significantly reduced, these are probably the most critical defects. Their size, geometry, and consequently their notch effect are randomly distributed across the sample surface, which is also reflected in a larger scatter. The smallest improvement is achieved by manual grinding (MG). The fatigue strength increases slightly from $\sigma_{a,200\,k} = 80$ MPa to 85 MPa. However, the S–N curve drops steeply ($k,MG = 0.4$) and the scatter is very wide ($TN,MG = 6.7$). In addition, more samples fractured in the clamping area and therefore outside the gage section, which is why these are not included in the evaluation. This is probably due to the fact that the material removal and the uniformity of the ground surface depends strongly on the skills of the operator.

Figure 7b shows the samples printed with an interruption of 10 h. In case of the as-built specimens, the fatigue strength decreases by 25% to $\sigma_{a,200\,k} = 60$ MPa due to the notch effect of the marks. The scatter of the values and the gradient of the S–N curve are similar for both sample types. Fatigue strength is significantly influenced by near-surface defects and inhomogeneities such as roughness, pores or geometric defects [13, 35–38]. The mark represents such a defect with a size of more than 100 µm and has a negative effect on the fatigue properties. Although the values of the not interrupted specimens are not achieved, the fatigue strength is significantly improved by the tested post-processing methods. Despite the fact that neither vibratory finishing nor blasting was able to remove the mark, the load amplitude that can be applied increased strongly by 62% after vibratory finishing and even 113% after blasting. The interruption marks were completely removed only by manual grinding. For this reason, it was expected that this method would generate the best results. However, the strength of $\sigma_{a,200\,k} = 101$ MPa is only slightly higher than that of the vibratory finished samples (97 MPa) and much lower compared to the blasted samples (128 MPa).

### 3.4 Fracture analysis

Figures 8 and 9 show the fracture locations of the fatigue specimens in relation to the interruption level, indicated by the red dashed line in Fig. 8 and markings in Fig. 9. Since the fracture behavior is identical for the three processing states AB, SB and VF, only the AB specimens are shown in Fig. 9 as a representative example. The regularly printed samples (NO) show a random and wide distribution of the fracture location. In contrast, for interrupted specimens (WITH), the as-built, the blasted as well as the vibratory finished specimens fail exclusively near the interruption level. Only the manually ground samples do not exhibit a distinct fracture pattern. Here, the influence of the individual post-processing method was evident. With blasting, a stationary condition is likely to be established after a sufficient processing time, which does not change significantly even after a longer processing time and which is independent of the operator. A completely different situation can be seen after manual grinding. Depending on the operator, the material removal and the uniformity of the reworked surface varies greatly. This is also reflected in the fracture behavior of the specimens. The random distribution of the fracture location suggests that the most critical effect of an interruption has been eliminated by the removal of the interruption marks. In addition to the marks, an increased porosity in the interlayer is another critical defect resulting from an interruption of a PBF-LB/M process as shown in **Error! Reference source not found.** b. For this reason, it was expected that the interruption level would remain the weak point of the manually ground samples and that a high proportion will still fail within this area. However, the random distribution of the fracture suggests that other effects appear to be more critical than the increased porosity in the interruption level. The uneven reworking creates local differences in roughness, residual stresses and, in some cases, significant differences in diameter within the gage section. In addition, defects close to the surface with random size and distribution are exposed, concealing the local effects of increased porosity in the interruption level. This effect is even greater for rotating bending test, since the bending stress increases toward the surface.

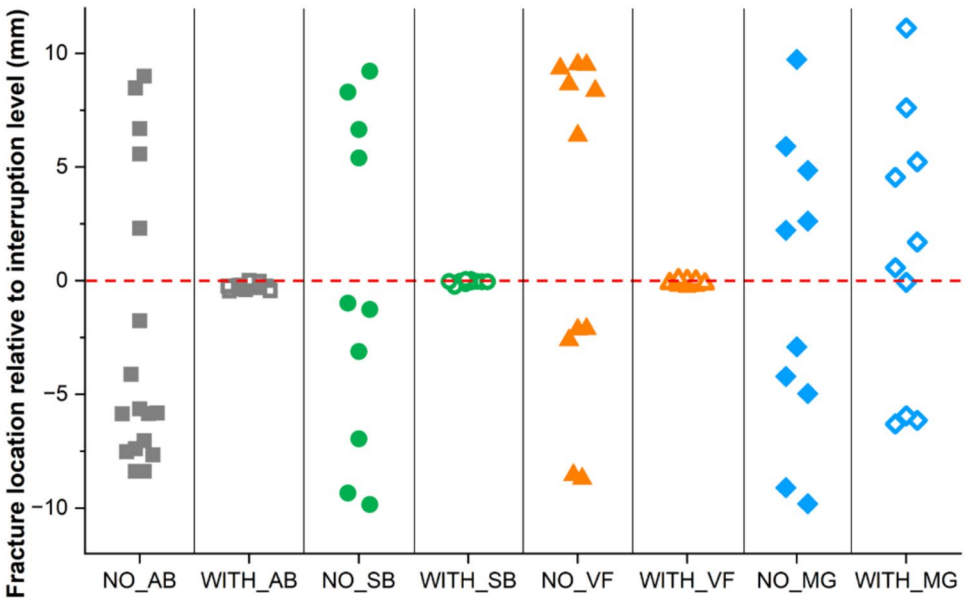


**Fig. 8** Fracture locations relative to the interruption level (dashed red line) for the investigated machining conditions

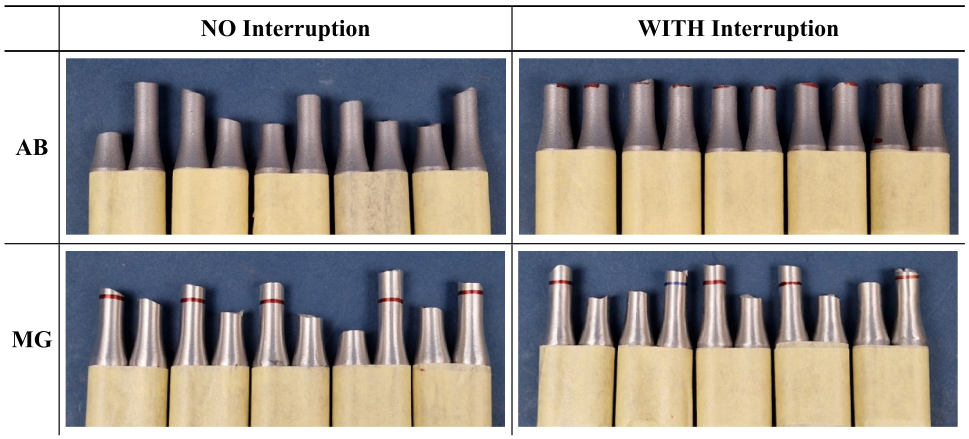


**Fig. 9** Fracture location of representative fatigue specimens printed without (NO) and with a process interruption (WITH) for the machining conditions as-built and manually ground. Blasted and vibratory finished samples show the same fracture pattern as the as-built samples

All regular as-built samples failed at single inhomogeneities directly at the surface (Fig. 10a). Numerous studies have proven that crack growth always starts from a defect at the surface due to the higher residual stresses [13, 30, 39, 40]. In contrast, several smaller defects are present on the surface of the interrupted as-built specimens, indicating an overall defective area, as also shown by Mahtabi et al. [11]. Figure 10b shows three exemplary defects that are close to each other. The many small defects merge and lead to premature failure of the samples. In general, the fracture surfaces of the interrupted samples show more and larger lack of fusion pores. These are attributed to the increased layer thickness as a result of an unsuitable restart procedure when continuing the build job.

Regardless of whether there was an interruption or not, the fracture in the blasted samples always starts from an inhomogeneity below the surface (Fig. 10c and d). However, other studies have found that even in the presence of large pores in the border area, defects always initiate cracks directly on the surface [39]. It is suspected that due to the compressive stresses in the surface area introduced by the post-processing methods, the critical region migrates toward the interior of the specimens where the compressive stresses gradually change back into residual tensile stresses. At the point where the stresses become large enough again and overlap with the stresses due to the load, the component fails at the next critical inhomogeneity. As was already evident in Fig. 5, the fine blasting beads even penetrate the fine corners of the mark, which greatly reduces its negative effect.

Despite the existing residual compressive stresses, the NO_VF samples primarily fail at a defect directly on the surface (Fig. 10e). These defects are probably the craters shown in Fig. 4. Since the roughness after vibratory finishing is quite low, these profile defects are now the most critical. For WITH_VF samples, on the other hand, the crack starts at the interruption mark and extends to defects nearby

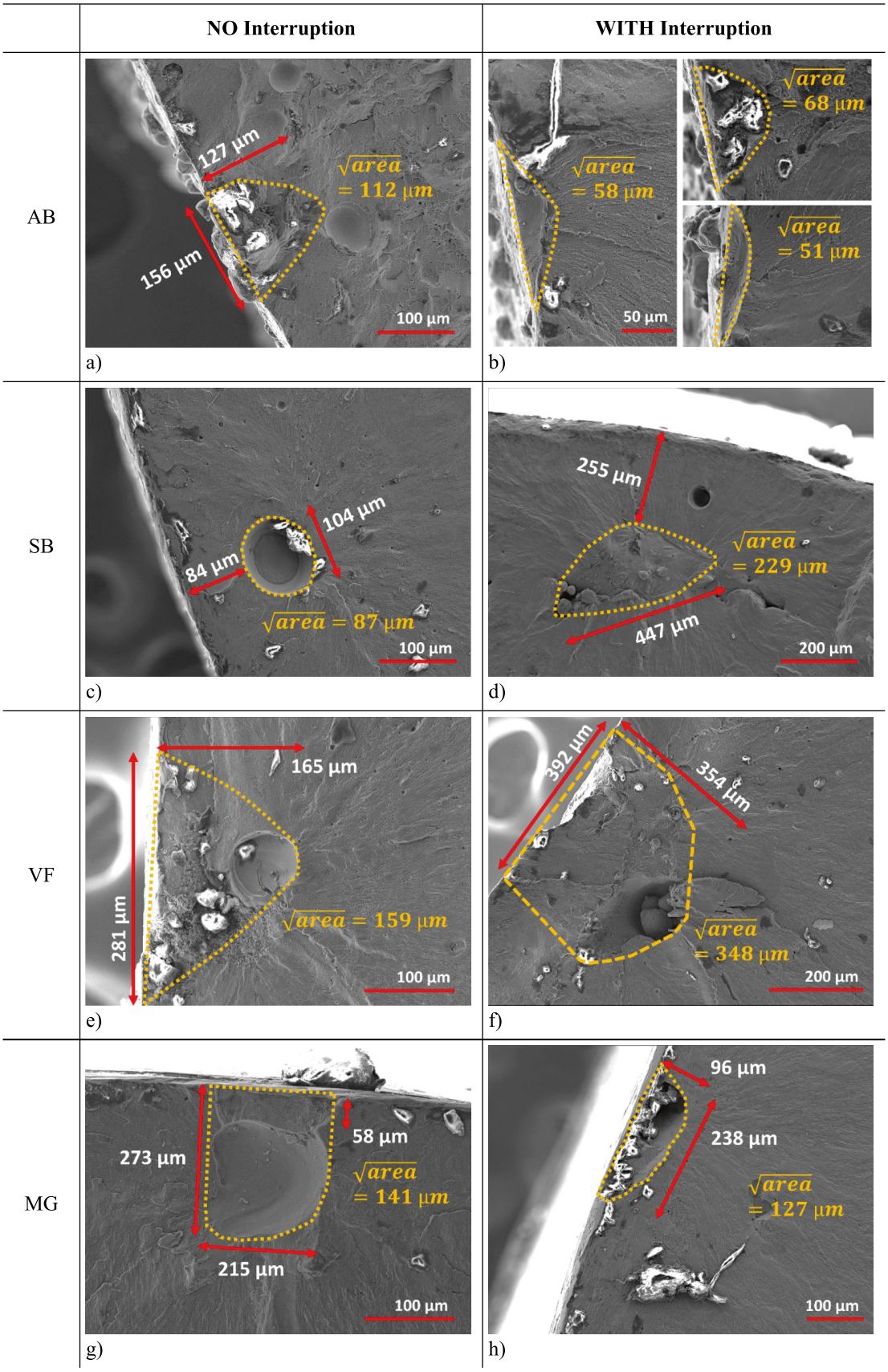


**Fig. 10** Exemplary locations, dimensions, and $\sqrt{area}$ according to Murakami [29] of fracture-causing defects

(Fig. 10f). Unlike blasting, where the fine particles can even reach the small edges and corners in the interruption marks, the abrasive media for vibratory finishing consist of triangles with approx. 10 mm in size. These large particles are unable to access the bottom of the surface craters as well as the small corners of the marks. This implies that the roughness and residual stress values in these areas might be similar to those of an as-built surface.

In case of the manually ground samples, the crack originates from defects close to the surface, which were apparently exposed during post-processing (Fig. 10g and h). This exposure of near-surface defects might provide a further explanation for the large scattering of the samples as the presence, size and location of these defects are purely coincidental.

Figure 11 shows the interruption mark visible in the fracture surface of a WITH_AB sample. The defect size can be estimated using Murakami's simplified method $\sqrt{10} * c$ where $c$ corresponds to the defect size [29]. This equation can be used to estimate the defect size of very shallow circumferential cracks and of the surface roughness. For the defect depth $c$, the size of the mark can be used. With an average of 100 µm and a maximum size of 145 µm, this results in a $\sqrt{area}$ of 316 to 459 µm, which is significantly larger than the usual defects, ranging from 51 µm to 348 µm (Fig. 10).

Figure 12 illustrates the distance between the fracture location and the interruption level in relation to the product of the defect size $\sqrt{area}$ and the shape factor $Y$ presented in Eq. 1. To be able to estimate the defect size range for each type, the crack-inducing defects of the samples with the lowest and the highest achieved fatigue life were measured. However, this does not mean that there are no samples with smaller or larger defects. The first noticeable aspect is the cluster formation. As can also be seen in Fig. 8, the fracture location of the regularly manufactured samples (NO) varies greatly, while the variants manufactured with an interruption (WITH) fail almost exclusively in the area near the interruption. Only one of the WITH_MG samples does not follow this pattern (highlighted by red circle). This might be due to the non-uniformity of the specimens. It can also be seen that the range of the defect sizes is significantly larger for the WITH samples than for the NO samples. This is probably due to the negative effect of the mark and the increased porosity in the interruption level. Furthermore, the WITH_AB samples show several smaller defects as shown in Fig. 10b. This makes it difficult to identify the most critical defect here. For comparison, the defect size of the interruption mark is shown as well. As this is a defect directly on the surface, a $Y$ of 0.65 was used. As shown earlier, the defect is significantly larger than the usual defects in regularly printed specimens. The mark is expected to influence not only the position but also the size of the crack initiating defect. Currently, their interaction is not well understood and cannot be considered in the evaluations (Fig. 12).

## 4 Conclusions

This study investigated the extent to which the consequences of a process interruption on PBF-LB/M AlSi10Mg components can be reduced using quick and easy post-processing methods. For this purpose, three methods were tested: blasting, vibratory finishing and manual grinding. These methods can all be used unplanned and without much preparation. Each of these methods offers different advantages and limitations, influencing the component properties in different ways. The investigations provide the following findings:

- The as-built samples show the rough surface known from numerous studies, which is due to the adhesion of incompletely melted powder particles. There are also craters on the surface which are probably due to roughness or profile valleys. Due to the high-temperature gradients in PBF-LB/M, residual tensile stresses are generated in the surface area of the as-built specimens. As a result of the interruption and the cooling of the system and the specimens, the interruption mark known from other studies was created, which significantly diminishes the fatigue strength. This corresponds to a notch approximately

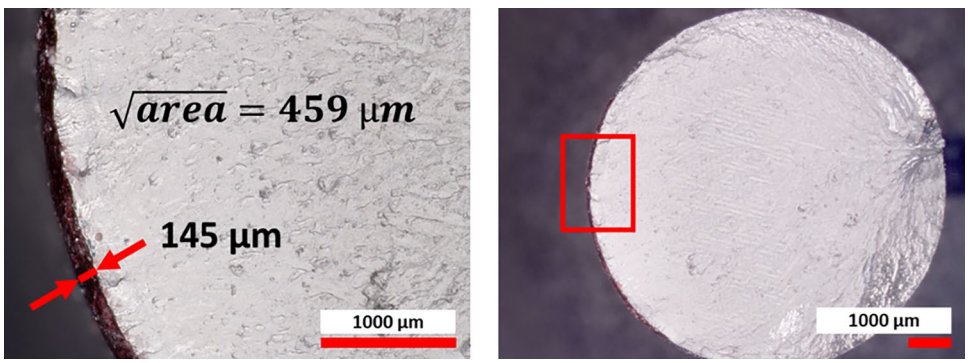


**Fig. 11** Example of an interruption mark visible in the fracture surface of a WITH_AB sample

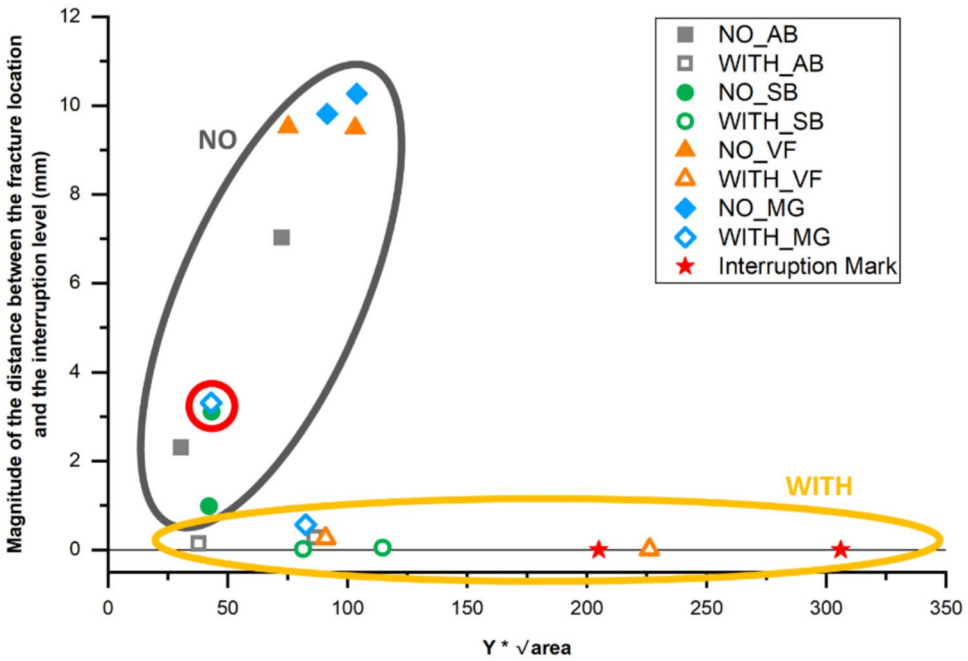


**Fig. 12** Distance between the fracture location and the interruption level as a function of the product of the defect size $\sqrt{area}$ and the factor Y (0.65 for surface defects; 0.5 for defects in the volume)

0.1 mm in size and has a preferred direction correlating with the gas flow, as also described in other studies. The regularly manufactured samples show a random distribution of the fracture location and the fracture triggering defect is always located directly on the surface. In contrast, the samples produced with an interruption fail exclusively in the interruption plane. In addition, the crack originates from several points on the surface and not from a single defect. This demonstrates the critical effect of a process interruption on the fatigue strength of as-built specimens.

- The loose adhering particles and roughness peaks are removed by blasting and vibratory finishing, which significantly improves the roughness. While the profile of the interruption marks is smoothed by these post-processing methods, the size is barely affected. Although the mark is not reduced, a considerable improvement in fatigue resistance is achieved. Even the strength values of the as-built samples printed without an interruption are surpassed. This is probably due to the residual compressive stresses present in the border area, indicating plastic deformation and hardening. These are higher after blasting than with vibratory finishing, resulting in the highest fatigue strength of the blasted samples. Both the blasted and vibratory finished specimens fail at random heights when printed regularly, but fail exclusively in the interruption level if the printing process is paused. In case of the blasted samples, the fracture originates from defects in the contour area below the surface. It is suspected that the residual compressive stresses at this point are very low or have even reverted to residual tensile stresses, so that a crack starts from the nearest defect.
- Manual grinding turned out to be the only way to completely remove the marks. However, the material removal and the uniformity of the reworked surface depend strongly on the person carrying out the work. In addition, pores close to the surface are exposed, acting as fracture-inducing defects. Their size, shape, and distribution in the samples are random, which is reflected in a large scatter of fatigue strength and the fracture location.

As the results show, the tested post-processing methods can be used to mitigate the negative effects after a process interruption in PBF-LB of AlSi10Mg. This is particularly relevant for long and time-critical build jobs and can help reduce the scrap rate. However, despite the general improvement in the strength level, the increased scattering of fatigue life has a negative effect on the performance of the components. The wider scatter is probably due to a higher layer thickness and thus increased porosity caused by an unsuitable procedure when continuing the build process. By optimizing the restart procedure, this defect could be reduced, thereby further minimizing the negative effects of a process interruption. This issue is part of current research and will be addressed in future publication.

**Acknowledgements** The author would like to thank Alexandra Widuch and Steffen Lübbecke (Institute of Weapons Technology and Materials Science, UniBwM) and Carsten Neukirchen (Institute of Chemical and Environmental Engineering, UniBwM) for their support and advice.

**Funding** Open Access funding enabled and organized by Projekt DEAL. As being part of the project FLAB-3Dprint this work was funded by dtec.bw®-Zentrum für Digitalisierungs- und Technologieforschung der Bundeswehr (dtecbw.de) and the European Union's program NextGenerationEU.

**Data availability** Depending on the scope, research data can be shared.

## Declarations

**Conflict of interest** For this research, there is no conflict of interest for all authors.



## References

1. Gockel J, Sheridan L, Koerper B, Whip B (2019) The influence of additive manufacturing processing parameters on surface roughness and fatigue life. Int J Fatigue 124:380–388. https://doi.org/10.1016/j.ijfatigue.2019.03.025
2. Vafadar A, Guzzomi F, Rassau A, Hayward K (2021) Advances in metal additive manufacturing: a review of common processes, industrial applications, and current challenges. Appl Sci. https://doi.org/10.3390/app11031213
3. VDI Verein Deutscher Ingenieure e.V., "Additive Fertigungsverfahren - Pulverbettbasiertes Schmelzen von Metall mittels Laserstrahl (PBF-LB/M) - Fehlerkatalog - Fehlerbilder beim Laser-Strahlschmelzen," (VDI 3405 Blatt 2.8). 2022–12–00, Vol. 25.030
4. Stoll P, Spierings A, Wegener K (2019) Impact of a process interruption on tensile properties of SS 316L parts and hybrid parts produced with selective laser melting. Int J Adv Manuf Technol 103:367–376. https://doi.org/10.1007/s00170-019-03560-1
5. Hammond V, Schuch M, Bleckmann M (2019) The influence of a process interruption on tensile properties of AlSi10Mg samples produced by selective laser melting. Rapid Prototyping J 25:1442–1452. https://doi.org/10.1108/RPJ-04-2018-0105
6. Binder M, Leong C, Anstaett C, Schlick G, Seidel C, Reinhart G (2020) Effects of process interruptions on the microstructure and tensile properties of AlSi10Mg parts manufactured by Laser-Based Powder Bed Fusion. Procedia CIRP 94:182–187. https://doi.org/10.1016/j.procir.2020.09.035
7. Terrazas CA, Mayoral FL, Garcia OF, Hossain MS, Espalin D, Fernandez A, Murr LE, Wicker RB (2021) Effects of process interruptions on microstructure and mechanical properties of three face centered cubic alloys processed by laser powder bed fusion. J Manuf Process 66:397–406. https://doi.org/10.1016/j.jmapro.2021.04.013
8. Richter J, Sajadifar SV, Niendorf T (2021) On the influence of process interruptions during additive manufacturing on the fatigue resistance of AlSi12. Add Manuf. https://doi.org/10.1016/j.addma.2021.102346
9. Stokes RM, Yadollahi A, Priddy MW, Bian L, Hammond VH, Doude HR (2022) Effects of build interruption and restart procedure on microstructure and mechanical properties of laser powder bed fusion Al-Si-10Mg. J Mater Eng Perform. https://doi.org/10.1007/s11665-022-07217-1
10. Richardsen S, Crawford GH, Gockel J (2023) Effect of a build pause on the fatigue behavior of laser powder bed fusion 316L stainless steel with as-built surfaces. Eng Fail Anal. https://doi.org/10.1016/j.engfailanal.2023.107590
11. Mahtabi M, Yadollahi A, Stokes R, Doude H, Priddy M (2023) Effect of build interruption during laser powder bed fusion process on structural integrity of Ti-6Al-4V. Eng Fail Anal. https://doi.org/10.1016/j.engfailanal.2023.107626
12. Moser M, Brenner S, Strauß L, Löwisch G, Nedeljkovic-Groha V (2024) Effect of a process interruption on the mechanical properties of AlSi10Mg components produced by laser powder bed fusion (PBF-LB/M). Prog Add Manuf. https://doi.org/10.1007/s40964-024-00641-w
13. Beevers E, Brandão AD, Gumpinger J, Gschweitl M, Seyfert C, Hofbauer P, Rohr T, Ghidini T (2018) Fatigue properties and material characteristics of additively manufactured AlSi10Mg – Effect of the contour parameter on the microstructure, density, residual stress, roughness and mechanical properties. Int J Fatigue 117:148–162. https://doi.org/10.1016/j.ijfatigue.2018.08.023
14. Avanzini A, Battini D, Gelfi M, Girelli L, Petrogalli C, Pola A, Tocci M (2019) Investigation on fatigue strength of sand-blasted DMLS-AlSi10Mg alloy. Procedia Struct Integ 18:119–128. https://doi.org/10.1016/j.prostr.2019.08.146
15. Strauß L, Löwisch G (2024) Effect of residual stress, surface roughness, and porosity on fatigue life of PBF-LB AlSi10Mg. Adv Struct Mater 203:275–290. https://doi.org/10.1007/978-3-031-49043-9
16. Damon J, Dietrich S, Vollert F, Gibmeier J, Schulze V (2018) Process dependent porosity and the influence of shot peening on porosity morphology regarding selective laser melted AlSi10Mg parts. Addit Manuf 20:77–89. https://doi.org/10.1016/j.addma.2018.01.001
17. Bagherifard S, Beretta N, Monti S, Riccio M, Bandini M, Guagliano M (2018) On the fatigue strength enhancement of additive manufactured AlSi10Mg parts by mechanical and thermal post-processing. Mater Des 145:28–41. https://doi.org/10.1016/j.matdes.2018.02.055
18. Maleki E, Bagherifard S, Unal O, Revuru M, Bandini M, Guagliano M (2023) The efficiency of tumble finishing as a final post-treatment for fatigue enhancement of notched laser powder bed fusion AlSi10Mg. Sci Rep. https://doi.org/10.1038/s41598-023-30660-6
19. Balla SK, Mallaiah M, Subramaniyan AK (2024) Effect of post-processing techniques on the surface roughness of laser powder bed fusion processed AlSi12 Alloy. Procedia Struct Integ 56:41–48. https://doi.org/10.1016/j.prostr.2024.02.035
20. Bhaduri D, Penchev P, Dimov S, Essa K, Carter LN, Pruncu CI, Jiang J, Pullini D (2020) On the surface integrity of additive manufactured and post-processed AlSi10Mg parts. Procedia CIRP 87:339–344. https://doi.org/10.1016/j.procir.2020.02.093
21. Nasab M, Giussani A, Gastaldi D, Tirelli V, Vedani M (2019) Effect of surface and subsurface defects on fatigue behavior of alsi10mg alloy processed by laser powder bed fusion (L-PBF). Metals. https://doi.org/10.3390/met9101063
22. Mesicek J, Ma Q-P, Hajnys J, Zelinka J, Pagac M, Petru J, Mizera O (2021) Abrasive surface finishing on SLM 316L parts fabricated with recycled powder. Appl Sci. https://doi.org/10.3390/app11062869

23. Uhlmann E, Fleck C, Gerlitzky G, Faltin F (2017) Dynamical fatigue behavior of additive manufactured products for a fundamental life cycle approach. Procedia CIRP 61:588–593. https://doi.org/10.1016/j.procir.2016.11.138
24. Lamagna L, Paiella A, Masi S, Bottini L, Boschetto A, Veniali F (2021) Selective laser melting process of al–based pyramidal horns for the W-band: fabrication and testing. Int J Infrared Millimeter Waves 42:154–173. https://doi.org/10.1007/s10762-020-00759-2
25. DIN Deutsches Institut für Normung e.V., "Prüfung metallischer Werkstoffe - Umlaufbiegeversuch," (DIN50113). 2018-12-00, Vol. 77.040.10
26. DIN Deutsches Institut für Normung e.V., "Geometrische Produktspezifikation (GPS) Oberflächenbeschaffenheit: Tastschnittverfahren: Regeln und Verfahren für die Beurteilung der Oberflächenbeschaffenheit," (EN ISO 4288:1997). 1998-04-00, Vol. 17.040.20
27. DIN Deutsches Institut für Normung e.V., "Zerstörungsfreie Prüfung – Röntgendiffraktometrisches Prüfverfahren zur Ermittlung der Eigenspannungen," (EN 15305). 2009-01-00, Vol. 19.100
28. DIN Deutsches Institut für Normung e.V., "Schwingfestigkeitsversuch – Durchführung und Auswertung von zyklischen Versuchen mit konstanter Lastamplitude für metallische Werkstoffproben und Bauteile," (DIN 50100). 2022-12-00, 19.060; 77.040.10
29. Murakami Y (2019) Metal Fatigue, 2nd edn. Elsevier
30. Aboulkhair NT, Maskery I, Tuck C, Ashcroft I, Everitt NM (2016) Improving the fatigue behaviour of a selectively laser melted aluminium alloy: Influence of heat treatment and surface quality. Mater Des 104:174–182. https://doi.org/10.1016/j.matdes.2016.05.041
31. Chan KS, Koike M, Mason RL, Okabe T (2012) Fatigue life of titanium alloys fabricated by additive laser manufacturing techniques for dental implants. Metall and Mater Trans A 44:1010–1022. https://doi.org/10.1007/s11661-012-1470-4
32. Grigoriev SN, Metel AS, Tarasova TV, Filatova AA, Sundukov SK, Volosova MA, Okunkova AA, Melnik YA, Podrabinnik PA (2020) Effect of cavitation erosion wear, vibration tumbling, and heat treatment on additively manufactured surface quality and properties. Metals. https://doi.org/10.3390/met10111540
33. Buchbinder D, Meiners W, Pirch N, Wissenbach K, Schrage J (2014) Investigation on reducing distortion by preheating during manufacture of aluminium components using selective laser melting. J Laser Appl. https://doi.org/10.2351/1.4828755
34. Li C, Liu ZY, Fang XY, Guo YB (2018) Residual stress in metal additive manufacturing. Procedia CIRP 71:348–353. https://doi.org/10.1016/j.procir.2018.05.039
35. Mower TM, Long MJ (2016) Mechanical behavior of additive manufactured, powder-bed laser-fused materials. Mater Sci Eng, A 651:198–213. https://doi.org/10.1016/j.msea.2015.10.068
36. Du Plessis A, Beretta S (2020) Killer notches: The effect of as-built surface roughness on fatigue failure in AlSi10Mg produced by laser powder bed fusion. Add Manuf. https://doi.org/10.1016/j.addma.2020.101424
37. Lai W-J, Li Z, Ohja A, Li Y, Forsmark J, Engler C, Su X (2020) Effects of surface roughness and porosity on fatigue behavior of alsi10mg produced by laser powder bed fusion process. Struct Integ Add Manuf Mater Parts. https://doi.org/10.1520/STP163120190127
38. Raja A, Cheethirala SR, Gupta P, Vasa NJ, Jayaganthan R (2022) A review on the fatigue behaviour of AlSi10Mg alloy fabricated using laser powder bed fusion technique. J Market Res 17:1013–1029. https://doi.org/10.1016/j.jmrt.2022.01.028
39. M. Moser, S. Brenner, L. Strauß, G. Löwisch and V. Nedeljkovic-Groha. 2022, Einfluss der PBF-LB/M-Prozessparameter auf Rauheit und Randporosität sowie die resultierende Lebensdauer zyklisch beanspruchter Bauteile aus AlSi10Mg, https://doi.org/10.48447/ADD-2022-004
40. Brandl E, Heckenberger U, Holzinger V, Buchbinder D (2012) Additive manufactured AlSi10Mg samples using Selective Laser Melting (SLM): microstructure, high cycle fatigue, and fracture behavior. Mater Des 34:159–169. https://doi.org/10.1016/j.matdes.2011.07.067